

Article

The Ultrasonic Polar Scan for Composite Characterization and Damage Assessment: Past, Present and Future [†]

Mathias Kersemans ^{1,*}, Arvid Martens ², Joris Degrieck ¹, Koen Van Den Abeele ², Steven Delrue ², Lincy Pyl ³, Filip Zastavnik ³, Hugo Sol ³ and Wim Van Paepegem ¹

¹ Mechanics of Materials and Structures, Department of Materials Science and Engineering, Ghent University, Technologiepark-Zwijnaarde 903, 9052 Zwijnaarde, Belgium; joris.degrieck@ugent.be (J.D.); wim.vanpaepegem@ugent.be (W.V.P.)

² Wave Propagation and Signal Processing, Department of Physics, KULeuven-KULAK, Etienne-Sabbelaan 52, 8500 Kortrijk, Belgium; arvid.martens@kuleuven-kulak.be (A.M.); koen.vandenabeele@kuleuven-kulak.be (K.V.D.A.); steven.delrue@kuleuven-kulak.be (S.D.)

³ Department Mechanics of Materials and Constructions, Vrije Universiteit Brussel, Pleinlaan 2, 1050 Brussels, Belgium; lincy.pyl@vub.ac.be (L.P.); filip.zastavnik@vub.ac.be (F.Z.); hugo.sol@vub.ac.be (H.S.)

* Correspondence: mathias.kersemans@ugent.be; Tel.: +32-9331-0427

[†] This paper is an extended version of paper published in the 6th International Conference on Emerging Technologies in Non-destructive Testing, ETNDT6 held in Brussels, 27–29 May 2015.

Academic Editors: Dimitrios G. Aggelis and Nathalie Godin

Received: 30 December 2015; Accepted: 14 February 2016; Published: 22 February 2016

Abstract: In the early 1980's, the ultrasonic polar scan (UPS) technique was developed to assess the fiber direction of composites in a nondestructive way. In spite of the recognition by several researchers as being a sophisticated and promising methodology for nondestructive testing (NDT) and materials science, little advance was made during the following 30 years. Recently however, the UPS technique experienced a strong revival and various modifications to the original UPS setup have been successfully implemented. This revival has exposed several powerful capabilities and interesting applications of the UPS technique for material characterization and damage assessment. This paper gives a short historical overview of the UPS technique for characterizing and inspecting (damaged) fiber-reinforced plastics. In addition, a few future research lines are given, which will further expand the applicability and potential of the UPS method to a broader range of (damaged) materials, bringing the UPS technique to the next level of maturity.

Keywords: ultrasound; ultrasonic polar scan; composites; NDT; characterization; damage

1. Introduction

An ultrasonic polar scan (UPS) is obtained by replacing the translational movement of a classical ultrasonic C-scan setup with a rotational movement. Hence, instead of scanning a plate surface at normal incidence, the UPS insonifies a certain material spot from as many oblique incidence angles ψ (ϕ, θ) as possible [1]. A schematic of the UPS method is presented in Figure 1a. Depending on the employed ultrasound, we speak of a pulsed ultrasonic polar scan (P-UPS) for a broadband pulse or a harmonic ultrasonic polar scan (H-UPS) for mono-frequency ultrasound. To improve coupling of the ultrasonic wave energy in the sample, the plate sample is immersed in water. Simply recording the transmitted (or reflected) ultrasound amplitude then yields a UPS image. Figure 1b,c shows current state-of-the-art P-UPS recordings for aluminum and $[0^\circ]_8$ carbon/epoxy (C/E) laminate, using an ultrasonic pulse with central frequency $f_c = 5$ MHz. The vertical incident angle θ is placed on

the radial axis, the in-plane polar angle φ is represented along the angular axis, while the assigned gray (or color) scale is a measure of the transmitted (or reflected) pulse amplitude. Hence, the P-UPS image comprises a large collection of amplitudes of obliquely transmitted (or reflected) ultrasound pulses.

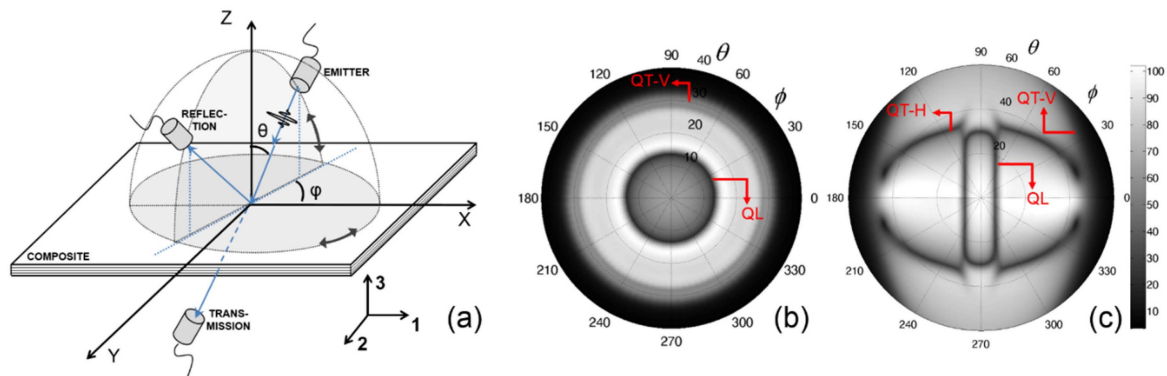


Figure 1. Schematic of ultrasonic polar scan (UPS) method (a). State-of-the-art pulsed ultrasonic polar scan (P-UPS) recordings at $f_c = 5$ MHz: aluminum with thickness $d = 0.6$ mm (b) and $[0^\circ]_8$ C/E laminate with thickness $d = 1.1$ mm (c). “QL”, “QT-H” and “QT-V” stand for quasi-longitudinal wave and quasi-transverse wave with horizontal and vertical polarization respectively.

Within the amplitude landscape of the P-UPS, characteristic contours emerge that more or less relate to the condition for critical (or in-plane) stimulation of the quasi-longitudinal, horizontally and vertically polarized quasi-transverse wave modes [2]. Note that along symmetry orientations, the prefix “quasi-” may be omitted, resulting in pure wave modes. These stimulation conditions are of course linked to the mechanical properties, like elasticity, of the insonified plate sample through Christoffel’s equation and Snell’s law [3,4]. As such, the P-UPS image actually represents an acoustic fingerprint of the mechanical properties. In the example of Figure 1b, the circular symmetry clearly puts on view the isotropic mechanical nature of the aluminum sample. The isotropic nature further invokes a degeneration of the quasi-transverse horizontal and quasi-transverse vertical wave, thus resulting in a P-UPS image with two characteristic contours. Figure 1c, on the other hand, displays a stretched appearance due to the unidirectional nature of the $[0^\circ]_8$ C/E laminate. Higher stiffness values lead to smaller critical angles (Snell’s law), and thus correspond to the contours being locally pressed inward in the P-UPS image. Considering the inner contour of Figure 1c, which is dominated by the quasi-longitudinally polarized wave, one can immediately determine that highest stiffness is found along $\varphi = 0^\circ$, which obviously corresponds to the orientation of the carbon reinforcement fibers of the $[0^\circ]_8$ C/E laminate.

In the remainder of this manuscript, a historical overview of the UPS research is given, starting from the initial results of the pioneering researchers, going over our recent advances [5], and finishing with currently investigated research lines.

2. The Past: 1981–2010

In the early 1980’s, the UPS technique was first introduced by Van Dreumel and Speijer in a pulsed version in order to assess the fiber orientation of composites [1]. The beauty of the intriguing patterns made the pioneering authors state [1]: “A library of Polar-patterns, stored as ‘fingerprints’, raises the possibility of laminate identification by pattern recognition”. It is unfortunate that in the following years, only one sequel study was performed by Van Dreumel and Speyer to further explore the capabilities of the ultrasonic polar scan [6].

It took fifteen years before the technique was investigated again through the work of Degrieck [7–9]. He used a modernized scanning system to obtain more accurate and detailed P-UPS experiments. The work of Degrieck has identified several practical applications of the P-UPS technique

for composite materials: (i) estimation of fiber direction; (ii) determination of fiber volume fraction and porosity and (iii) detection of fatigue damage [8,9]. In addition, he and Van Leeuwen implemented a numerical procedure for simulating P-UPS images of homogeneous composites [7], in view of bringing the technique to the next level: full quantitative characterization of the elastic properties of composite materials using a mixed experimental-numerical approach. Although the gap between experiment and simulation was not yet bridged, their numerical results did contribute to the physical understanding of the formation of a P-UPS image. They found that the characteristic patterns are (more or less) a representation of critical bulk wave angles, while the global transmission amplitude exposes attenuation properties [8]. Consequently, a P-UPS image may be used for characterizing viscoelastic material properties.

The ultrasonic polar scan research has been further extended by Declercq, first as a student of Degrieck [2,10,11] and afterwards as a professor at the Georgia Institute of Technology in Metz [12]. He applied the technique for detecting tension-tension induced fatigue damage in glass fiber composites by tracing shifts in the characteristic fingerprint [10]. In addition, Declercq extended the simulation technique towards layered viscoelastic materials having arbitrary anisotropy using a global matrix method [2,11]. He experimentally implemented a time-of-flight (TOF) version of the P-UPS method and commented on the superior sensitivity (compared with amplitude recording) to the presence of damage features [12]. Here, TOF is defined as the arrival time of the peak amplitude of the transmitted ultrasound pulse. As an illustration, Figure 2 displays state-of-the-art amplitude and TOF landscape of a P-UPS for a $[0^\circ]_8$ C/E laminate [13].

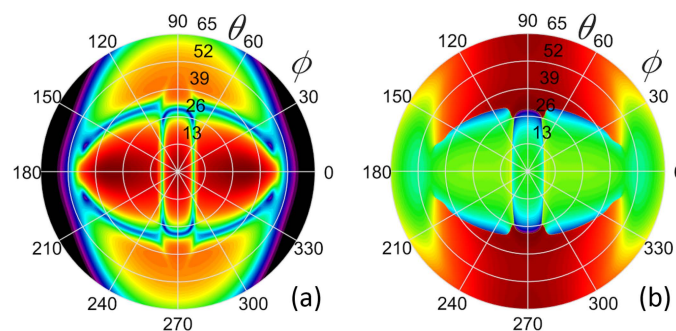


Figure 2. P-UPS for $[0^\circ]_8$ C/E laminate: amplitude (a) and time-of-flight (TOF) (b) landscape [13].

It is clear from the above results that the UPS technique already had several applications, but it is evenly clear that many capabilities and opportunities still have to be explored.

3. The Present: 2010–2015

Building further on this background, Kersemans intensified the research on the ultrasonic polar scan method in 2010 [13]. Several barriers were identified that impede the further development of the UPS methodology. Three main barriers may be summarized as:

- lack of high quality experimental data,
- lack of a computationally efficient simulation model, and
- lack of adequate inverse modeling techniques to couple experiment to simulation.

3.1. The Ultrasonic Polar Scan Revisited

The experimental barrier has been tackled by the development of a 5-axis scanner that records ultrasonic polar scans in a fully automated way. During recording a UPS experiment, the scanner typically insonifies a material spot from more than 1,000,000 different incidence angles ψ (ϕ, θ) in a timeframe of ~ 15 min. High-precision encoders are installed, providing accurate position feedback for the insonification direction. The USIP40 (General Electric, Hurm (Efferen), Germany), with a sampling

clock of 400 MHz, is used as pulser/receiver apparatus. With this setup, we identified several pitfalls in the earlier experimental procedures, which prevented the correct and accurate recording of an ultrasonic polar scan [14]. The high quality of our experiments can already be seen in Figure 1b,c, showing P-UPS recordings for aluminum and $[0^\circ]_8$ C/E laminate.

Secondly, a simulation technique has been implemented to support experimental observations [15]. The simulation model is founded on a transfer matrix technique [16–18], and allows the simulation of UPS for immersed layered viscoelastic anisotropic media. A Fourier-based approach is employed to account for the spectral nature of the considered pulsed ultrasonic wave. As all transducers show some deviation from their design conditions, the recorded output signal (in water) of the actual transducer is directly used as input for the simulation model. In Figure 3, an example is displayed for a broadband transducer, which shows a clear deviation from its designed central frequency $f_c = 5$ MHz.

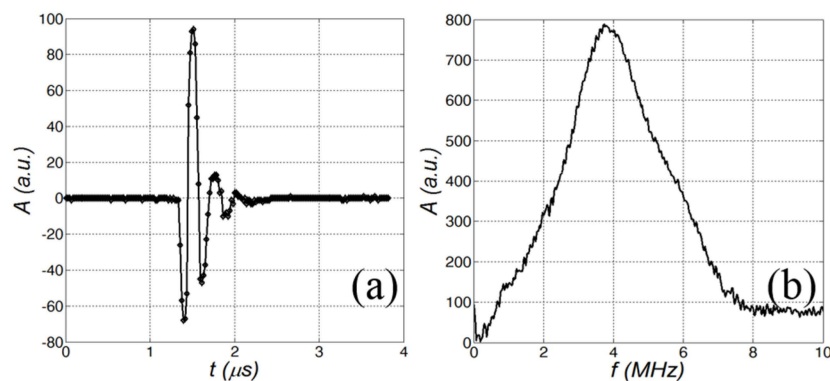


Figure 3. Excitation signal of a 5-MHz broadband transducer: temporal (a) and frequency (b) domain. The spectral content clearly reveals a central frequency around 4 MHz, instead of 5 MHz.

Compared to previous simulation models, we significantly reduced the computational time. Typically, the simulation time for a UPS is in the order of seconds. Figure 4a,b displays the simulated P-UPS of the aluminum plate and the $[0^\circ]_8$ C/E laminate. As realistic material properties for immersion liquid and solid were considered, and the experimental broadband pulse of Figure 3 was explicitly modeled, the P-UPS simulations in Figure 4 may be straightforwardly compared with the P-UPS experiments displayed in Figure 1b,c. It is clear that a good visual comparison is obtained between experiment and simulation.

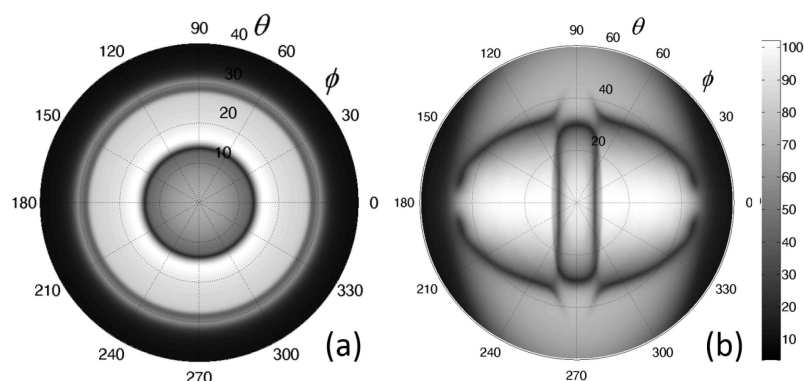


Figure 4. P-UPS simulation (ultrasound pulse of Figure 3 is used as input) for aluminum (a) and $[0^\circ]_8$ C/E laminate (b).

This brings us to the third barrier, which is tackled by implementing an inversion procedure to couple experiment to simulation, in view of identifying material parameters. Basically, the simulated

P-UPS image is fitted to the recorded P-UPS image while updating the material properties by means of a genetic algorithm [13,19,20]. The obvious goal is to find a set of viscoelastic material parameters that minimizes the difference between both amplitude landscapes. A schematic of the optimization procedure is shown in Figure 5a. Figure 5b shows the optimized result for the $[0^\circ]_8$ C/E laminate in terms of the viscoelastic tensor $C_{ij} = C_{ij}^R - iC_{ij}^I$, with C_{ij}^R representing the elastic properties and C_{ij}^I the attenuation characteristics.

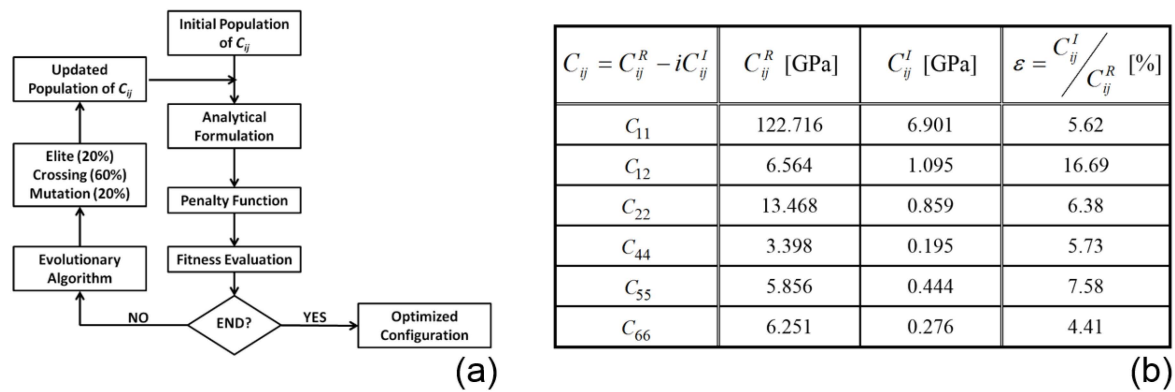


Figure 5. Schematic of inversion procedure to identify composite properties (a) and identified properties for $[0^\circ]_8$ C/E laminate (b) [13,19]. (a) reproduced from [19], Copyright Society for Experimental Mechanics, 2014.

In this way, the (visco)elastic properties for a range of (composite) materials have been identified, showing good correspondence with alternative identification techniques [13,19]. Apart from the obtained successes, we still encountered some drawbacks and difficulties with an inversion procedure that is based on amplitude data only. For this reason we are currently implementing a more robust inversion procedure that accounts for both the TOF and amplitude landscape of a P-UPS recording (further details in Section 4.1) [21,22].

3.2. Extensions of UPS Method

During our investigations, we found that additional information is encoded in the ultrasonic polar scan recordings. In the following, we briefly indicate a few of the various extensions that were implemented over the last few years.

3.2.1. Harmonic Ultrasonic Polar Scan

Numerical simulations suggested that the global view of a UPS image is not only a function of material parameters, but also strongly depends on the (temporal) shape of the employed ultrasound wave [2]. This has led us to the experimental and numerical investigation of a harmonic version of the ultrasonic polar scan (H-UPS) [15]. In Figure 6, a comparison is shown between P-UPS (broadband wave with central frequency $f_c = 5$ MHz) and H-UPS (harmonic wave with frequency $f = 5$ MHz) recordings of a $[0^\circ]_8$ C/E laminate. Apart from the similar global view, imposed by the unidirectional nature of the scanned sample, one observes that the H-UPS image has a “richer” fingerprint.

Contrary to the P-UPS image, the patterns in the H-UPS image depend on the exact ultrasonic frequency. This is easily understood considering that the H-UPS image puts on view the stimulation condition of dispersive, *i.e.*, frequency dependent, Lamb waves, while the P-UPS image is mainly governed by bulk wave characteristics [2,15,23].

For the case of harmonic signals, the UPS analysis was extended to the evaluation of both the amplitude and the phase signal of the transmitted wave. In this way, knowledge can be obtained about the complex transmission coefficient. Figure 7 displays the H-UPS images for a $[0^\circ]_8$ C/E laminate,

considering the analysis of both the amplitude and the phase of the transmission signal. Note that the sharp discontinuities in the phase map are a mere consequence of phase wrapping.

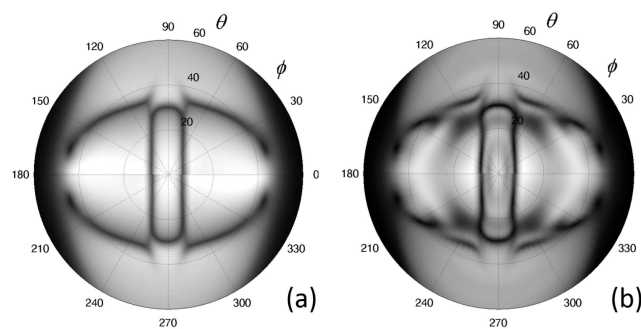


Figure 6. Experimental recordings of a $[0^\circ]_8$ C/E laminate: P-UPS at $f_c = 5$ MHz (a) and harmonic ultrasonic polar scan (H-UPS) at $f = 5$ MHz (b).

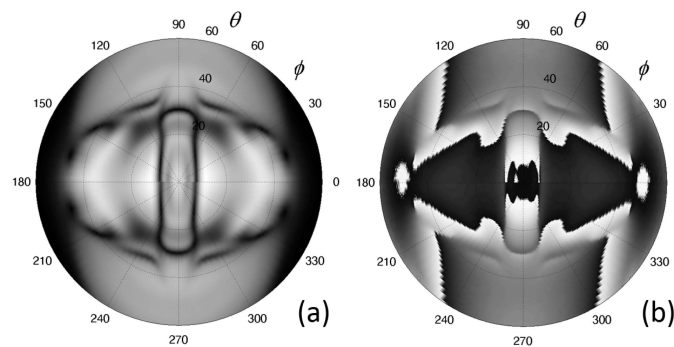


Figure 7. H-UPS recordings for $[0^\circ]_8$ carbon/epoxy laminate at $f = 5$ MHz: amplitude (a) and phase (b) analysis.

3.2.2. Ultrasonic Backscatter Polar Scan (UBPS)

During our UPS investigations, we persistently observed a small amount of ultrasonic energy being backscattered to the emitter, even for large incident angles θ . Recording of the backscattered signal according to the UPS principle then results in an ultrasonic backscatter polar scan (UBPS). Depending on the employed wave, we speak of P-UBPS for ultrasonic pulses [24] and H-UBPS for quasi-harmonic ultrasound [25] (similarly as done for H-UPS and P-UPS). A schematic of the UBPS method, together with a H-UBPS recording for a $[0^\circ]_8$ C/E laminate, is presented in Figure 8.

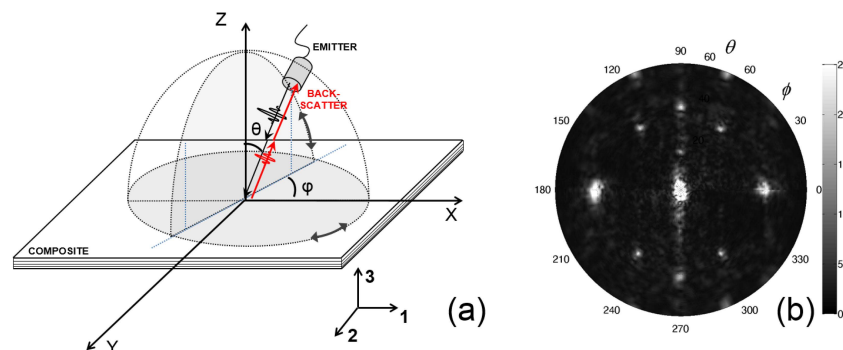


Figure 8. Schematic of ultrasonic backscatter polar scan (UBPS) method (a) and harmonic ultrasonic backscatter polar scan (H-UBPS) recording for a $[0^\circ]_8$ C/E laminate (b).

Typically, a H-UBPS image is characterized by well-defined high amplitude backscatter spikes, which can be linked to diffraction phenomena under the Bragg condition [25–28]. As such, these spikes directly expose geometrical characteristics of (sub)surface structures. For the $[0^\circ]_8$ C/E laminate, the observed backscatter spikes originate at the imprint left by the peel-ply cloth during manufacturing of the laminate [24].

3.3. Applications of UPS and UBPS

The UPS and the UBPS, both in pulsed and harmonic version, have been applied to a range of nondestructive testing (NDT) applications involving polymeric, metallic and fiber-reinforced materials.

3.3.1. Static Damage

Various fiber-reinforced plastics have been quasi-statically loaded to induce material degradation. In Figure 9a,b, P-UPS images are shown before and after (quasi-)static shear loading of a $[-45^\circ, +45^\circ]_S$ C/E laminate. The indicated overlap angle ζ provides a measure of the angle between the orientation of the fiber reinforcement. Initially $\zeta = 91.5^\circ$, indicating that the stacking of the laminate was not perfect (see Figure 9a). After loading in shear, the overlap angle reduces to $\zeta = 81.5^\circ$ (see Figure 9b), which thus reveals a shift in fiber orientation of 10° . Figure 9c shows the fracture area of a $[-45^\circ, +45^\circ]_S$ C/E laminate loaded in shear until failure, indeed displaying a very large shift in fiber orientation. The evolution of the overlap angle ζ was monitored for a range of shear load levels, and we found a clear relationship between the applied shear load level and the observed shift in fiber orientation in the P-UPS images [29].

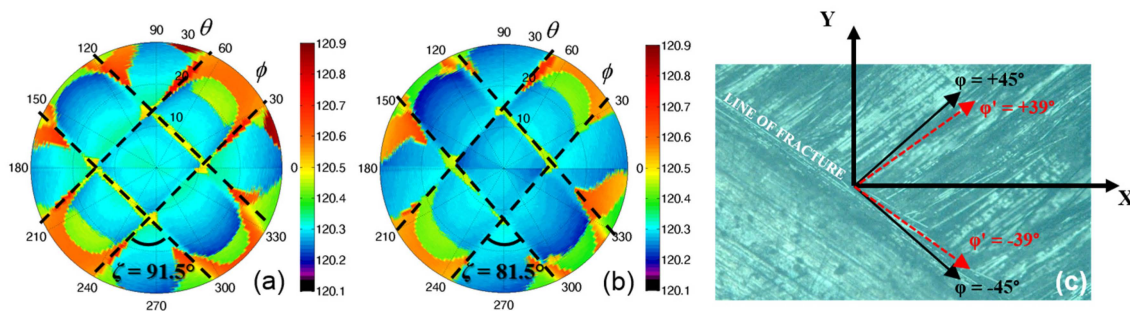


Figure 9. P-UPS images of $[-45^\circ, +45^\circ]_S$ C/E laminate: before (a) and after (b) applying the shear load. Microscopic image of the fracture area when shear loading a $[-45^\circ, +45^\circ]_S$ C/E laminate until failure (c).

3.3.2. Delamination

As the patterns in a H-UPS image are governed by the stimulation conditions for Lamb waves, these patterns must shift position in the presence of a delamination. This is easily understood considering that a delamination divides the original laminate in two sub-laminates, resulting in different boundary conditions. Different boundary conditions invoke different Lamb wave stimulation conditions, and as such yield different H-UPS images [15,30]. This is demonstrated in Figure 10 for a cross-ply $[0^\circ, 90^\circ]_S$ C/E laminate (thickness $d = 1.1$ mm) provided with water-filled delaminations (with nominal thickness $D = 50$ μm) at different depth positions. Note that such types of delaminations are in general difficult to assess in thin composites using conventional normal incident ultrasonic techniques. Figure 10 clearly shows that the depth position of the delamination is well represented in the H-UPS images. Figure 10d further indicates that the H-UPS can even detect multiple overlapping water-filled delaminations.

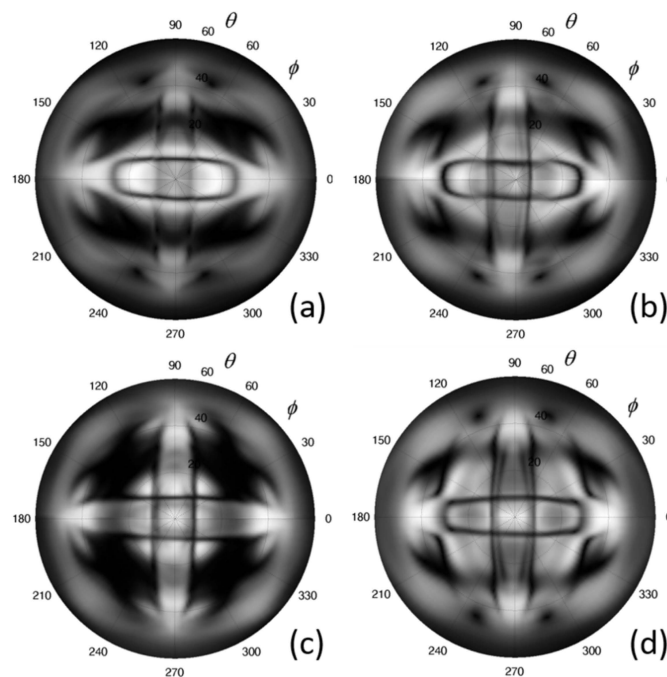


Figure 10. H-UPS recordings of a cross-ply C/E laminate at $f = 5$ MHz: $[0^\circ,90^\circ,90^\circ,0^\circ]$ (a); $[0^\circ,W,90^\circ,90^\circ,0^\circ]$ (b); $[0^\circ,90^\circ,W,90^\circ,0^\circ]$ (c) and $[0^\circ,W,90^\circ,90^\circ,W,0^\circ]$ (d). “W” stands for the position of the water-filled delamination.

Excellent agreement is obtained between the results of experiment and simulation. Further, our numerical computations indicate the ability of the H-UPS to characterize delamination parameters such as depth position and delamination thickness D . Currently, an inversion model is being implemented to extract these delamination parameters in an automated way.

3.3.3. Fatigue Damage

The UPS method was also applied to fatigued composites. Fatigue loading typically leads to the initiation, progression and accumulation of micro defects. At the macroscopic level, these defects manifest themselves in a directional reduction of the stiffness properties [31,32]. Such a directional stiffness reduction is visible as a stretching (along the direction of loading) of the UPS contours. This is explicitly demonstrated in Figure 11 for a woven C/E laminate (ultimate tensile strength of 770 MPa), which was fatigued along $\phi = 0^\circ$: 314,111 load cycles with stress range 0–625 MPa at a frequency of 5 Hz [33]. The P-UPS experiment yielded a stiffness reduction of 12.8% along the loading direction, which is in good agreement with extensometer data yielding a stiffness reduction of 11% [33].

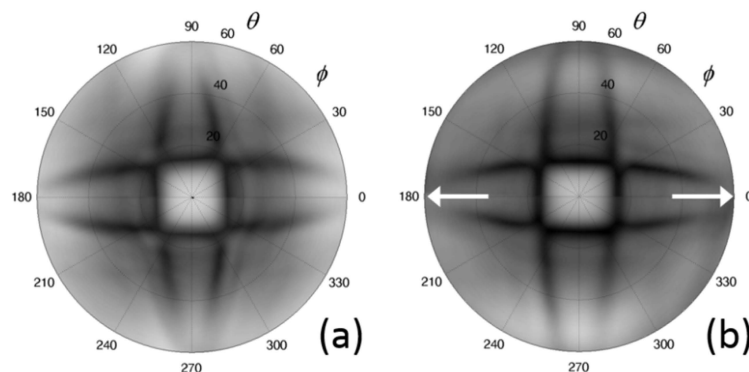


Figure 11. P-UPS recording of woven C/E laminate: before (a) and after (b) applying tension fatigue.

3.3.4. (Sub)surface Corrugation

As the characteristics of a periodic (sub)surface structure determine the position of the observed backscatter spikes in a H-UBPS experiment (see Figure 8b), we may also reverse this: start from a H-UBPS experiment and reconstruct the parameters of the periodic (sub)surface structure. A 2D subsurface corrugation has been applied to a polycarbonate sample through laser ablation. A microscopic image of the 2D corrugation is displayed in Figure 12a. The corresponding H-UBPS experiment at $f = 5$ MHz is shown in Figure 12b. Several well-defined backscatter spikes can be observed, which were used to reconstruct the in-plane parameters of the 2D corrugation. We obtained excellent agreement between the ultrasonic reconstruction, design parameters and optical measurement of the corrugation parameters (see Table 1).

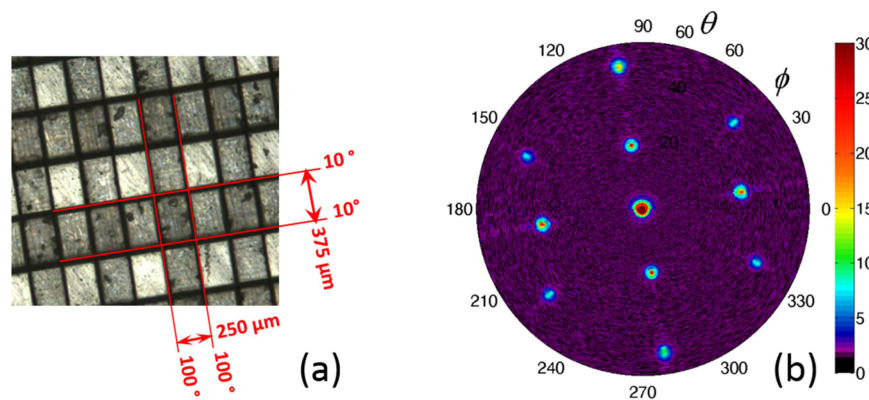


Figure 12. Microscopic image of ablated 2D subsurface corrugation (a) and corresponding H-UBPS recording at $f = 5$ MHz (b).

Table 1. Corrugation parameters: design (column 1), ultrasonic reconstruction (column 2) and optical measurement (column 3).

Corrugation Parameters	Design Values	Ultrasonic Reconstruction	Optical Measurement
Λ_1	250 μm	249.8 μm	250.1 μm
Φ_1	100°	99.3°	99.2°
Λ_2	375 μm	375.3 μm	374.8 μm
Φ_2	10°	9°	9.1°

The above method has also been applied to periodic subsurface structures having superimposed geometrical randomness. Although additional scattering features, such as Lyman and Rowland “ghosts” and “grass” [34,35], emerge in the H-UBPS image, we were still able to extract the basic corrugation parameters with excellent accuracy [13].

3.3.5. Strain Measurement

As the H-UBPS method is capable of reconstructing a periodic (sub)surface structure with excellent accuracy, it should also be feasible to detect any change in surface parameters due to strain. Instead of machining a periodic surface structure, which would mechanically weaken the sample, we simply exploit residual surface roughness features. The ultrasonic strain measurement technique has been demonstrated on cold-rolled DC06 steel coupons, which have a deterministic surface structure left from skin passing of the work rolls (see Figure 13). The surface structure has an average roughness $R_a = 1.1 \mu\text{m}$ with standard deviation $\sigma_{R_a} = 0.0502 \mu\text{m}$, and has a clear degree of aperiodic features superimposed. The DC06 steel samples have been plastically strained at different levels ranging from 2% up to 35%. One can clearly observe a positional shifting of the backscatter spikes when strained (see Figure 14), from which the applied in-plane strain field was reconstructed [36].

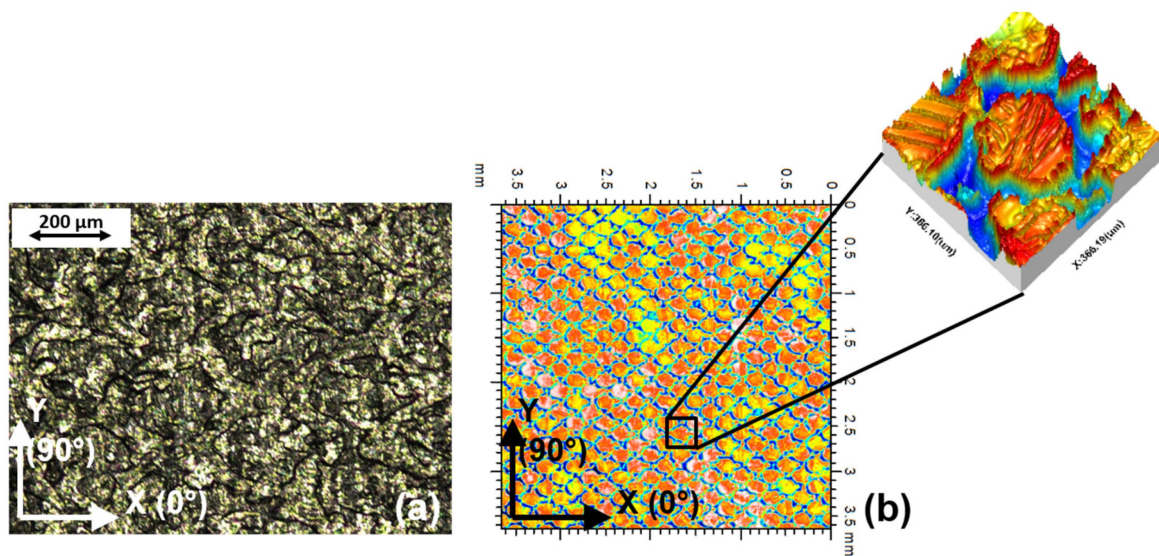


Figure 13. Optical visualization of the surface structure of DC06 steel: standard 2D microscopy (a) and 3D coherence correlation interferometry (after processing) (b).

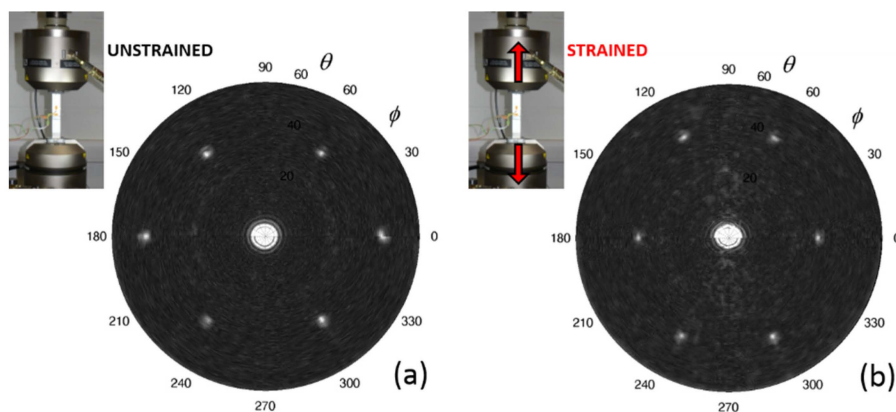


Figure 14. H-UBPS for DC06 steel coupon at $f = 5$ MHz: unstrained (a) and strained (b) state.

In addition, we also analyzed the response of ultrasonic broadband pulses at normal incidence, in order to detect any change in the stimulation condition of a thickness resonance (Lamb wave cut-off frequency). From this change, the out-of-plane strain component can then easily be obtained. The ultrasonically obtained strain values have been confronted with the results of conventional strain measurements techniques (manual micrometer, mechanical extensometer, mono- and stereovision digital image correlation), showing excellent agreement for a wide range of applied strain values [36]. Interestingly, the developed ultrasonic strain gauge is the only method that was able to determine a 3D local strain field in a single-sided and contactless manner.

4. The (Near) Future: 2015–...

The above results illustrate we are on the right track in advancing the U(B)PS technique towards a higher level of maturity. But, of course there are still open (research) questions to be tackled. In addition, more applications and novel approaches for materials science and non-destructive testing lie ahead. Several of these opportunities are, or will further be, investigated by the present authors.

4.1. Viscoelastic Tensor

The complex C-tensor identification scheme discussed in Section 2 is a procedure solely based on the analysis of the amplitude P-UPS landscape. That system identification procedure has its merits, but still suffers from drawbacks. First, the amplitude-based inversion procedure is ill-defined for samples with a high degree of viscoelasticity. Further, for certain materials, small discrepancies between the characteristic patterns and the critical bulk wave angles were observed [19], thus requiring special care during inversion. Finally, the current amplitude-based inversion is unable to provide the complete set of orthotropic viscoelasticity parameters.

Other researchers have already tried to tackle the problem of (visco)elastic tensor determination by considering TOF (and amplitude) analysis of obliquely incident waves [37–40]. Unfortunately, their approaches also have inherent limitations. As they consider only a limited set of orientation angles φ , prior knowledge about the material symmetry axes is required [37,40,41]. Secondly, those inversion schemes often rely on bulk wave approximations, which has the consequence that the plate thickness d should match the ultrasound frequency f . Thirdly, phase effects at the liquid-solid and solid-liquid interface are often ignored, though some authors incorporated the phase effect by considering an additional iterative step [38].

One of our current research lines is trying to reconcile the above two inversion procedures, *i.e.*, combining the analysis of amplitude P-UPS landscape with TOF analysis, in order to obtain a robust, stable and widely applicable procedure for extracting viscoelastic material parameters. In order to reach this goal, we consider a two-step inversion approach [21,22]. The schematic roadmap of this approach is presented in Figure 15. First, the elastic properties are extracted on the basis of the TOF landscape of a P-UPS recording. Second, damping parameters are obtained through analysis of the amplitude landscape of a P-UPS recording.

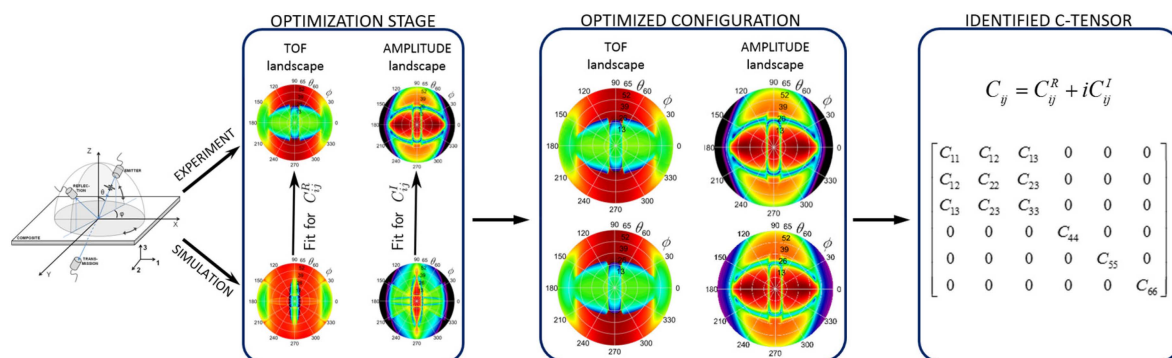


Figure 15. Roadmap for the identification of viscoelastic C-tensor using both TOF and amplitude P-UPS landscapes.

As the forward P-UPS simulation model (both amplitude and TOF) accounts for the true physical parameters, its validity is not restricted by the bulk wave approximation. Further, the optimization procedure includes a wide range of incidence angles $\Psi(\varphi, \theta)$, which makes prior knowledge about material symmetry ubiquitous. Finally, the large amount of redundant data will without doubt lead to robust and stable inversion results, even for noisy data. As such, we believe that our current effort may lead to a comprehensive approach in obtaining viscoelastic parameters for a wide range of (orthotropic) materials. As a matter of fact, we already successfully tested this system identification procedure for synthetic data [21,22], and we are now in the stage of applying this procedure to real experimental data.

4.2. Nonlinear U(B)PS

Until now, linear wave phenomena were used in the U(B)PS methodology for detecting, assessing and analyzing a range of damage features [24,29,30,33]. However, it is well-known from literature

that nonlinear wave phenomena show an increased sensitivity to early stage damage features as well as to certain classes of contact defects [42–45]. For this reason, the present authors are currently upgrading the U(B)PS methodology towards the nonlinear regime. One approach is to perform two experiments with different amplitude levels or with inverted wave amplitudes, and to investigate the lack of scalability which is typical for nonlinear features. Subtraction of both experiments (after scaling to the input excitation) then provides a measure of the presence of nonlinearity. Another approach is to combine U(B)PS with spectroscopic analysis. In that way, we can easily evaluate and analyze the U(B)PS images at various harmonics of the input frequency. Our first experimental results of the nonlinear version of the U(B)PS are very promising, and indicate a great potential for inspection of damaged (fiber-reinforced) materials. To validate the experimental results, we will also develop the corresponding simulation models that account for these nonlinear wave phenomena.

4.3. Redesign of UPS Scanner

As we realize that our current laboratory scanner does not meet in-field requirements, we are in the process of designing a portable UPS scanner. The current status of our portable scanner is presented in Figure 16. This device is made from mechanical parts and will only serve as an intermediate step as our final goal is to exclude any mechanical movement by using advanced phased matrix technology [46].



Figure 16. Current design of portable UPS scanner.

4.4. Comprehensive Inspection Approach

Most industrial-scale composite components are subject to a range of (accidental) loading conditions (fatigue, impact . . .), which lead to specific macroscopic damage phenomena (stiffness reduction, delamination . . .). Further considering the complex geometry (bends, stiffeners . . .) of typical engineering structures, it is clear that not a single non-destructive technique provides an objective and complete screening of the structural health of the investigated component. For this reason, the present authors are working towards a stepwise procedure in which various complementary inspection methods are applied. The first stage will involve a global testing of the component using for example, high-frequency modal analysis, in order to check for any deviations from the reference state [47,48]. Assuming there is an indication of anomalous response, the component will be further interrogated and inspected by more advanced and thorough techniques such as (lock-in) thermography and/or thermoelastic stress analysis [49–51], active shearography [51] and laser Doppler vibrometry [52]. These techniques actually provide a semi-quantitative view of the structural health of the component, and will identify “hotspots” that may deserve further attention. Finally, these identified “hotspots” will be investigated with local methods, like the UPS, in order to gain quantitative insight into the local damage state and/or local material properties.

5. Conclusions

This paper gives a short historical overview of the ultrasonic (backscatter) polar scan research for composite characterization and NDT. After introducing the pioneering results of the initiators, state-of-the-art research results are given and discussed. Various applications have been explicitly illustrated for a range of (fiber-reinforced) materials, including

- (Visco)elastic C-tensor identification through the use of inverse methods.
- Assessment of (quasi-)static shear damage in cross-ply C/E laminate.
- Detection of (overlapping) delamination in thin cross-ply C/E laminate.
- Assessment of tension-tension fatigue damage in woven C/E laminate.
- Identification of the in-plane parameters of 2D (sub)surface corrugation.
- Single-sided identification of a local 3D plastic strain field in DC06 steel coupon.

Final notes are given about our ongoing exploration of several novel and high-potential research lines, which will undoubtedly further advance the ultrasonic (backscatter) polar scan technique, bringing the methodology to its next level of maturity.

Acknowledgments: M.K. acknowledges the financial support of Bijzonder Onderzoeksfonds BOF (special research fund grant BOF.PDO.2015.0028.01). The authors further acknowledge the financial support of Fonds voor Wetenschappelijk Onderzoek FWO—Vlaanderen (grants FWO.G012010N and FWO.G0B9515N).

Author Contributions: M.K. conceived, designed and performed the experiments; M.K. and A.M. implemented the numerical models; L.P., F.Z., H.S. and S.D. provided samples; W.V.P., J.D. and K.V.D.A. supervised the presented research; M.K. wrote the paper.

Conflicts of Interest: The authors declare no conflict of interest.

References

1. Van Dreumel, W.H.M.; Speijer, J.L. Non-destructive composite laminate characterization by means of ultrasonic polar-scan. *Mater. Eval.* **1981**, *39*, 922–925.
2. Declercq, N.F.; Degrieck, J.; Leroy, O. Simulations of harmonic and pulsed ultrasonic polar scans. *NDT E Int.* **2006**, *39*, 205–216. [[CrossRef](#)]
3. Rokhlin, S.I.; Chimenti, D.E.; Nagy, P.B. *Physical Ultrasonics of Composites*; Oxford University Press: Oxford, UK, 2011.
4. Rose, J.L. *Ultrasonic Waves in Solid Media*; Cambridge University Press: Oxford, UK, 1999.
5. Kersemans, M.; Martens, A.; Delrue, S.; van den Abeele, K.; Pyl, L.; Zastavnik, F.; Sol, H.; Degrieck, J.; van Paepegem, W. The ultrasonic polar scan: Past, Present and future. In Proceedings of the Emerging Technologies in NonDestructive Testing (ETNDT6), Brussels, Belgium, 27–29 May 2015; pp. 133–139.
6. Van Dreumel, W.H.M.; Speijer, J.L. Polar-scan, a non-destructive test method for the inspection of layer orientation and stacking order in advanced fiber composites. *Mater. Eval.* **1983**, *41*, 1060–1062.
7. Degrieck, J.; van Leeuwen, D. Simulatie van een Ultrasonie Polaire Scan van een Orthotrope Plaat (in Dutch). In Proceedings of the 3rd Belgian National Congress on Theoretical and Applied Mechanics, Liege, Belgium, 30–31 May 1994.
8. Degrieck, J. Some possibilities of nondestructive characterisation of composite plates by means of ultrasonic polar scans. In Proceedings of the Emerging technologies in nondestructive testing (ETNDT), Patras, Greece, 22–23 May 1995; pp. 225–235.
9. Degrieck, J.; Declercq, N.F.; Leroy, O. Ultrasonic polar scans as a possible means of non-destructive testing and characterisation of composite plates. *Insight* **2003**, *45*, 196–201. [[CrossRef](#)]
10. Declercq, N.F.; Degrieck, J.; Leroy, O. On the influence of fatigue on ultrasonic polar scans of fiber reinforced composites. *Ultrasonics* **2004**, *42*, 173–177. [[CrossRef](#)] [[PubMed](#)]
11. Declercq, N.F.; Degrieck, J.; Leroy, O. Ultrasonic polar scans: Numerical simulation on generally anisotropic media. *Ultrasonics* **2006**, *45*, 32–39. [[CrossRef](#)] [[PubMed](#)]
12. Satyanarayan, L.; Weide, J.M.V.; Declercq, N.F. Ultrasonic polar scan imaging of damaged fiber reinforced composites. *Mater. Eval.* **2010**, *68*, 733–739.
13. Kersemans, M. Combined experimental-numerical study to the ultrasonic polar scan for inspection and characterization of (damaged) anisotropic materials. Ph.D. Thesis, Ghent University, Ghent, Belgium, 31 October 2014.
14. Kersemans, M.; van Paepegem, W.; van den Abeele, K.; Pyl, L.; Zastavnik, F.; Sol, H.; Degrieck, J. Pitfalls in the experimental recording of ultrasonic (backscatter) polar scans for material characterization. *Ultrasonics* **2014**, *54*, 1509–1521. [[CrossRef](#)] [[PubMed](#)]

15. Kersemans, M.; Martens, A.; van den Abeele, K.; Degrieck, J.; Pyl, L.; Zastavnik, F.; Sol, H.; van Paepegem, W. The quasi-harmonic ultrasonic polar scan for material characterization: Experiment and numerical modeling. *Ultrasonics* **2015**, *58*, 111–122. [[CrossRef](#)] [[PubMed](#)]
16. Rokhlin, S.I.; Wang, L. Stable recursive algorithm for elastic wave propagation in layered anisotropic media: Stiffness matrix method. *J. Acoust. Soc. Am.* **2002**, *112*, 822–834. [[CrossRef](#)] [[PubMed](#)]
17. Tan, E.L. Hybrid compliance-stiffness matrix method for stable analysis of elastic wave propagation in multilayered anisotropic media. *J. Acoust. Soc. Am.* **2006**, *119*, 45–53. [[CrossRef](#)] [[PubMed](#)]
18. Tan, E.L. Stiffness matrix method with improved efficiency for elastic wave propagation in layered anisotropic media. *J. Acoust. Soc. Am.* **2005**, *118*, 3400–3403. [[CrossRef](#)]
19. Kersemans, M.; Martens, A.; Lammens, N.; van den Abeele, K.; Degrieck, J.; Zastavnik, F.; Pyl, L.; Sol, H.; van Paepegem, W. Identification of the elastic properties of isotropic and orthotropic thin-plate materials with the pulsed ultrasonic polar scan. *Exp. Mech.* **2014**, *54*, 1121–1132. [[CrossRef](#)]
20. Kersemans, M.; Lammens, N.; Luyckx, G.; Degrieck, J.; van Paepegem, W. Quantitative measurement of the elastic properties of orthotropic composites by means of the ultrasonic polar scan method. *JEC Compos.* **2012**, *75*, 48–52.
21. Martens, A.; Kersemans, M.; Degrieck, J.; van Paepegem, W.; Delrue, S.; van den Abeele, K. Time-of-flight recorded pulsed ultrasonic polar scan for elasticity characterization of composites. In Proceedings of the Emerging Technologies in NonDestructive Testing (ETNDT6), Brussels, Belgium, 27–29 May 2015.
22. Van den Abeele, K.; Martens, A.; Kersemans, M.; Degrieck, J.; Delrue, S.; van Paepegem, W. Characterization of visco-elastic material parameters by means of the ultrasonic polar scan method. In Proceedings of the Acoustical Society of America—Fall 2015 Meeting, Jacksonville, FL, USA, 2–6 November 2015.
23. Kersemans, M.; Lammens, N.; Degrieck, J.; van den Abeele, K.; Pyl, L.; Zastavnik, F.; Sol, H.; van Paepegem, W. Extraction of bulk wave characteristics from a pulsed ultrasonic polar scan. *Wave Motion* **2014**, *51*, 1071–1081. [[CrossRef](#)]
24. Kersemans, M.; van Paepegem, W.; Lemmens, B.; van den Abeele, K.; Pyl, L.; Zastavnik, F.; Sol, H.; Degrieck, J. The pulsed ultrasonic backscatter polar scan and its applications for NDT and material characterization. *Exp. Mech.* **2014**, *54*, 1059–1071. [[CrossRef](#)]
25. Kersemans, M.; van Paepegem, W.; van den Abeele, K.; Pyl, L.; Zastavnik, F.; Sol, H.; Degrieck, J. Ultrasonic characterization of subsurface 2D corrugation. *J. Nondestruct. Eval.* **2014**, *33*, 438–442. [[CrossRef](#)]
26. De Billy, M.; Cohentenoudji, F.; Jungman, A.; Quentin, G.J. Possibility of assigning a signature to rough surfaces using ultrasonic backscattering diagrams. *IEEE Trans. Sonics Ultrason.* **1976**, *23*, 356–363. [[CrossRef](#)]
27. De Billy, M.; Quentin, G. Measurement of the periodicity of internal surfaces by ultrasonic testing. *J. Phys. D Appl. Phys.* **1982**, *15*, 1835–1841. [[CrossRef](#)]
28. Herbison, S.W. Ultrasonic diffraction effects on periodic surfaces. Ph.D. Thesis, Georgia Institute of Technology, Atlanta, GA, USA, August 2011.
29. Kersemans, M.; de Baere, I.; Degrieck, J.; van den Abeele, K.; Pyl, L.; Zastavnik, F.; Sol, H.; van Paepegem, W. Nondestructive damage assessment in fiber reinforced composites with the pulsed ultrasonic polar scan. *Polym. Test.* **2014**, *34*, 85–96. [[CrossRef](#)]
30. Kersemans, M.; Martens, A.; van den Abeele, K.; Degrieck, J.; Pyl, L.; Zastavnik, F.; Sol, H.; van Paepegem, W. Detection and localization of delaminations in thin carbon fiber reinforced composites with the ultrasonic polar scan. *J. Nondestruct. Eval.* **2014**, *33*, 522–534. [[CrossRef](#)]
31. Giancane, S.; Panella, F.W.; Dattoma, V. Characterization of fatigue damage in long fiber epoxy composite laminates. *Int. J. Fatigue* **2010**, *32*, 46–53. [[CrossRef](#)]
32. Taheri-Behrooz, F.; Shokrieh, M.M.; Lessard, L.B. Residual stiffness in cross-ply laminates subjected to cyclic loading. *Compos. Struct.* **2008**, *85*, 205–212. [[CrossRef](#)]
33. Kersemans, M.; de Baere, I.; Degrieck, J.; van den Abeele, K.; Pyl, L.; Zastavnik, F.; Sol, H.; van Paepegem, W. Damage signature of fatigued fabric reinforced plastic in the pulsed ultrasonic polar scan. *Exp. Mech.* **2014**, *54*, 1467–1477. [[CrossRef](#)]
34. Lyman, T. An explanation of the false spectra from diffraction gratings. *Proc. Am. Acad. Arts Sci.* **1903**, *39*, 39–47. [[CrossRef](#)]
35. Gale, H.G. Rowland ghosts. *Astrophys. J.* **1937**, *85*, 49–61. [[CrossRef](#)]

36. Kersemans, M.; Allaer, K.; van Paepegem, W.; van den Abeele, K.; Pyl, L.; Zastavnik, F.; Sol, H.; Degrieck, J. A novel ultrasonic strain gauge for single-sided measurement of a local 3D strain field. *Exp. Mech.* **2014**, *54*, 1673–1685. [[CrossRef](#)]
37. Castaings, M.; Hosten, B.; Kundu, T. Inversion of ultrasonic, plane-wave transmission data in composite plates to infer viscoelastic material properties. *NDT E Int.* **2000**, *33*, 377–392. [[CrossRef](#)]
38. Wang, L.; Lavrentyev, A.I.; Rokhlin, S.I. Beam and phase effects in angle-beam-through-transmission method of ultrasonic velocity measurement. *J. Acoust. Soc. Am.* **2003**, *113*, 1551–1559. [[CrossRef](#)] [[PubMed](#)]
39. Lavrentyev, A.I.; Rokhlin, S.I. Determination of elastic moduli, density, attenuation, and thickness of a layer using ultrasonic spectroscopy at two angles. *J. Acoust. Soc. Am.* **1997**, *102*, 3467–3477. [[CrossRef](#)]
40. Cawley, P.; Hosten, B. The use of large ultrasonic transducers to improve transmission coefficient measurements on viscoelastic anisotropic plates. *J. Acoust. Soc. Am.* **1997**, *101*, 1373–1379. [[CrossRef](#)]
41. Castellano, A.; Foti, P.; Fraddosio, A.; Marzano, S.; Piccioni, M.D. Mechanical characterization of CFRP composites by ultrasonic immersion tests: Experimental and numerical approaches. *Compos. B Eng.* **2014**, *66*, 299–310. [[CrossRef](#)]
42. Aymerich, F.; Staszewski, W.J. Impact damage detection in composite laminates using nonlinear acoustics. *Compos. A Appl. Sci. Manuf.* **2010**, *41*, 1084–1092. [[CrossRef](#)]
43. Scalerandi, M.; Gliozzi, A.S.; Bruno, C.L.E.; van den Abeele, K. Nonlinear acoustic time reversal imaging using the scaling subtraction method. *J. Phys. D Appl. Phys.* **2008**, *41*, 1–10. [[CrossRef](#)]
44. Meo, M.; Polimeno, U.; Zumpano, G. Detecting damage in composite material using nonlinear elastic wave spectroscopy methods. *Appl. Compos. Mater.* **2008**, *15*, 115–126. [[CrossRef](#)]
45. Hirsekorn, S.; Rabe, U.; Arnold, W. Characterisation and evaluation of composite materials by nonlinear ultrasonic transmission measurements. In Proceedings of the International Congress on Ultrasonics (ICU 2007), Wenen, Oostenrijk, 10–12 April 2007.
46. Drinkwater, B.W.; Wilcox, P.D. Ultrasonic arrays for non-destructive evaluation: A review. *NDT E Int.* **2006**, *39*, 525–541. [[CrossRef](#)]
47. Rucka, M. Damage detection in beams using wavelet transform on higher vibration modes. *J. Theor. Appl. Mech.* **2011**, *49*, 399–417.
48. Baba, B.O.; Thoppul, S.; Gibson, R.F. Experimental and numerical investigation of free vibrations of composite sandwich beams with curvature and debonds. *Exp. Mech.* **2010**, *51*, 857–868. [[CrossRef](#)]
49. Pitarresi, G. Lock-in signal post-processing techniques in infra-red thermography for materials structural evaluation. *Exp. Mech.* **2013**, *55*, 667–680. [[CrossRef](#)]
50. Wong, A.K.; Rajic, N.; Nguyen, Q. 50th anniversary article: Seeing stresses through the thermoelastic lens—A retrospective and prospective from an Australian viewpoint. *Strain* **2015**, *51*, 1–15. [[CrossRef](#)]
51. Hung, Y.Y.; Chen, Y.S.; Ng, S.P.; Liu, L.; Huang, Y.H.; Luk, B.L.; Ip, R.W.L.; Wu, C.M.L.; Chung, P.S. Review and comparison of shearography and active thermography for nondestructive evaluation. *Mater. Sci. Eng. R Rep.* **2009**, *64*, 73–112. [[CrossRef](#)]
52. Klepka, A.; Pieczonka, L.; Staszewski, W.J.; Aymerich, F. Impact damage detection in laminated composites by non-linear vibro-acoustic wave modulations. *Compos. B Eng.* **2014**, *65*, 99–108. [[CrossRef](#)]

